Sedimentary Geology 381 (2019) 65–75

Contents lists available at ScienceDirect

Sedimentary Geology

journal homepage: www.elsevier.com/locate/sedgeo

Conservative behavior of Mg isotopes in massive dolostones: From diagenesis to hydrothermal reworking

Zhongya Hu [a], Wenxuan Hu [a,b,*], Chuan Liu [a], Funing Sun [a], Yongli Liu [c], Weiqiang Li [a,**]

[a] State Key Laboratory for Mineral Deposits Research, School of Earth Sciences and Engineering, Nanjing University, Nanjing, Jiangsu 210093, China
[b] Institute of Energy Sciences, Nanjing University, Nanjing, Jiangsu 210093, China
[c] Northwest Exploration and Production Company, SINOPEC, Xinjiang, Urumqi 830011, China

ARTICLE INFO

Article history:
Received 19 October 2018
Received in revised form 19 December 2018
Accepted 20 December 2018
Available online 27 December 2018

Editor: Dr. B. Jones

Keywords:
Dolomite
Dolomitization
Magnesium isotopes
Homogeneous

ABSTRACT

Mg isotopes in syndepositional dolomite have been suggested to be a potential proxy for understanding seawater chemistry. However, it is argued that the δ^{26}Mg values of dolomite could be complicated by the effects of early diagenesis and later hydrothermal activities. Further investigations into the behaviors of Mg isotopes in dolomitization systems are needed to resolve this controversy. In the present study, we investigated early Ordovician dolostones from the Tarim Basin, including diagenetically altered dolomites, hydrothermally altered dolomites and well-preserved dolostones that precipitated in the slope, margin and interior of a carbonate platform. Different types of dolomites, bulk dolostone and limestone were sampled by microdrilling for analyses of C-O-Mg isotope compositions and REE concentrations. The dolostone δ^{13}C values match those of coeval seawater, and the REE distribution patterns in the dolostones are comparable with those in the limestones, indicating that the dolostones originated from syndiagenetic dolomitization. The δ^{26}Mg values of the various syndiagenetic dolomites that formed in the slope, margin and interior of the carbonate platform are similar, averaging approximately $-2.06‰ \pm 0.20‰$. No stratigraphic variability in the dolomite Mg isotopes can be discerned, which implies that the Mg isotope compositions of the porewater were homogeneous during massive dolomitization and remained in equilibrium with seawater. Additionally, the δ^{26}Mg values of the altered dolostone do not show correlations with diagenetic and hydrothermal signals, demonstrating that dolomite Mg isotopes are insensitive to postdepositional alteration. Given these facts, we propose that Mg isotopes in dolostones have conservative behaviors during diagenesis and late stage hydrothermal reworking.

1. Introduction

Magnesium is an important component in seawater, and seawater Mg isotope signature can respond to changes in marine environments (Higgins and Schrag, 2015; Li et al., 2015; Huang et al., 2016; Gothmann et al., 2017; Bialik et al., 2018). Magnesium isotope compositions of calcite have been demonstrated to be sensitive to resetting at conditions of deep-burial diagenesis (Riechelmann et al., 2016; Rollion-Bard et al., 2016; Mavromatis et al., 2017). By contrast, dolomite is an important sink of Mg in global Mg cycles (Wilkinson and Algeo, 1989), and Mg isotopes in dolomite are more robust against deep-burial diagenesis (Geske et al., 2012; Azmy et al., 2013; Hu et al., 2017). It has been suggested that dolomite is a potential archive of seawater δ^{26}Mg for inferring the Mg cycling in the geological history (Li et al., 2015; Hu et al., 2017).

Sedimentary dolomite is commonly regarded as the product of diagenesis in soft sediments rather than the direct precipitation from seawater (Warren, 2000). The δ^{26}Mg values in dolomite have been interpreted to be principally controlled by porewater chemistry during early diagenesis (Higgins and Schrag, 2012; Fantle and Higgins, 2014; Blättler et al., 2015; Chanda and Fantle, 2017). Studies of modern dolomitization processes in different sedimentary and diagenetic settings have shown that evolutionary patterns of porewater chemistry vary in different types of early diagenetic systems due to changes in hydrologic conditions, resulting in stratigraphic variations in Mg isotope compositions in carbonates (Ahm et al., 2018; Higgins et al., 2018). For example, the δ^{26}Mg values of recent sabkha dolomites in tidal flats of Abu Dhabi are similar to those of seawater (Geske et al., 2015b). In contrast, the Neogene dolomites in a lagoon in Little Bahama Bank had adequate Mg isotope exchange with seawater with a $\Delta^{26}Mg_{dolomite\text{-}seawater}$ of approximately $-2.0‰$ (Higgins et al., 2018). Generally, the current understandings on the variation of dolomite Mg isotope compositions in dolomitization are mainly from observations of relatively young dolomitization systems. However, the widely distributed dolostones in the Mesozoic-Paleozoic formed via massive dolomitization, for which

* Correspondence to: W. Hu, Institute of Energy Sciences, Nanjing University, Nanjing, Jiangsu 210093, China.
** Corresponding author.
E-mail addresses: huwx@nju.edu.cn (W. Hu), liweiqiang@nju.edu.cn (W. Li).

https://doi.org/10.1016/j.sedgeo.2018.12.007
0037-0738/

there is no genuine analog in modern marine environments (Warren, 2000). Although the porewater of the ancient dolomitization system has vanished, the Mg isotopes in the dolomite are preserved and can be analyzed precisely. It is necessary to study the response of dolomite Mg isotopes to massive dolomitization processes and to re-evaluate the potential of dolomite Mg isotopes as proxies of ancient seawater chemistry.

The Tarim Basin is a large shallow carbonate platform in the Sinian-Ordovician and developed thick-bedded dolostones from the late Cambrian to the Early Ordovician (Gao and Fan, 2014, 2015). Based on paleogeography reconstructions for this region, the shallow carbonate platform can be subdivided into several sedimentary subenvironments, including the interior, margin, and slope, which have systematic differences in diurnal temperature variation, sedimentation rate, and hydrodynamic conditions (Gao and Fan, 2014, 2015; Guo et al., 2016; Du et al., 2018). The early Ordovician Penglaiba Formation is a typical massive dolostone sequence that is widely exposed in the basin (Guo et al., 2016; Du et al., 2018), providing an excellent case to study Mg isotope behaviors during the dolomitization process. Additionally, previous studies have shown that hydrothermal activities that were associated with early Permian volcanisms superimposed on the Penglaiba Formation, and the origin and geochronology of the hydrothermal fluids, and the processes of fluid-rock interactions in this region have been well documented (Dong et al., 2013; Guo et al., 2016; Jia et al., 2016; Du et al., 2018). As a result, the hydrothermally altered dolostones in Penglaiba Formation provide an ideal natural laboratory for investigation of the behaviors of dolomite Mg isotopes in hydrothermal reworking processes.

In this study, we sampled bulk dolostones of the Penglaiba Formation from the Aksu outcrop and three drilling cores (YB5, S88 and TS2). We used microdrilling to extract different types of dolomite with different textures from polished hand specimens. Magnesium isotope analyses were complemented by analyses of C-O isotopic compositions, rare earth element (REE) concentrations and petrographic features to constrain the relations between post-depositional processes and Mg isotope variabilities. Our results indicate that the different types of syndiagenetic dolomites deposited in different sedimentary settings have uniform δ^{26}Mg values of $-2.06‰ \pm 0.20‰$, implying that chemistry of the porewater was buffered by coeval seawater during the dolomitization processes irrespective of sedimentary settings. Furthermore, the results suggest that post-depositional processes, including diagenetic and hydrothermal alterations, did not induce notable changes in the Mg isotope signals in the dolomite.

2. Geological setting and samples

The Tarim Basin is located in northwestern China and is surrounded by the Kunlun-Altyn Mountains to the south and the Tianshan Mountains to the north (Fig. 1A) (Lin et al., 2015). From the Sinian to Middle Ordovician, the Tarim Basin was dominated by a shallow carbonate platform, on which thick-bedded carbonates deposited (Gao and Fan, 2014, 2015) (Fig. 1B). Paleomagnetic studies indicated that Tarim Basin located near the equator from late Cambrian to early Ordovician (Nie, 1991), and the regional climate was arid and hot (Trotter et al., 2008; Munnecke et al., 2010), causing evaporation of seawater and widespread intensive dolomitization in the carbonate platform (Guo et al., 2016; Du et al., 2018). The upper Cambrian and lower Ordovician strata, including the Qiulitage Group, Penglaiba Formation and lower Yingshan Formation, are mainly composed of dolostones (Guo et al., 2016; Jia et al., 2016). Conodont biostratigraphy and carbon isotope stratigraphy studies indicate that the Penglaiba Formation in Tarim Basin formed during the Tremadocian (~485 Ma) of early Ordovician (Zhang and Munnecke, 2016). According to sedimentary studies and 2D seismic data, in early Ordovician, the northern and central parts of the Tarim Basin were semi-closed interior platforms, whereas the Aksu area in the western basin and Hetian area in the southeastern basin were dominated by deep sea environments, and the transition areas between the platform and deep seas were margins and slopes around the carbonate platform (Gao and Fan, 2014, 2015) (Fig. 1A). At the end of the early Permian, widespread volcanism occurred in the Tarim Basin (Lin et al., 2015). 2D seismic profiles and outcrops indicate that the lower Paleozoic massive carbonate layers are cut by fractures and faults (Lin et al., 2015), which acted as efficient conduits for hydrothermal fluids (Dong et al., 2013; Jia et al., 2016).

In this study, four representative profiles that located in the northern Tarim Basin, Aksu area and Hetian area were selected, and samples were collected from three drill cores (S88, TS2 and YB5) and an outcrop (Aksu) (Fig. 1A). According to the reconstruction of sedimentary environments in Tarim Basin in the early Ordovician, the marine carbonates in these profiles were deposited in the slope (Aksu outcrop), margin (YB5 core) and interior (S88 and TS2 core) of the carbonate platform respectively (Gao and Fan, 2014, 2015; Guo et al., 2016) (Fig. 1A). To systematically study the Mg isotope behaviors of dolomites in syndepositional and postdepositional processes, diagenetically altered dolomites, hydrothermally altered dolomites and well-preserved dolostones in Penglaiba Formation were sampled. Based on detailed microscopic observations, different types of dolomite in hand specimens were sampled with a microdrill for chemical and isotopic analyses. Coeval limestones were also collected and analyzed.

3. Methods

3.1. Petrography and mineral analyses

Fifty-five thin sections were prepared from samples for polarized and cathodoluminescence microscopy. Cathodoluminescence microscopy was performed on a cold-cathode instrument (type CL8200-MK5) with an acceleration voltage of 13–14 kV, a current of 250–300 mA, and a chamber pressure of 0.03 to 0.05 mBar.

3.2. Geochemical analyses

3.2.1. Trace element analysis

Twenty-four bulk carbonate samples were selected for the trace element analysis (Appendix Table S5). Fifty milligrams of carbonate powder was weighed and digested in 5 ml 4.5 N HNO_3 in a Teflon beaker. Hydrofluoric acid was not used to avoid digestion of detrital components in the samples. Then, the solution was dried at 99 °C on a hotplate and redissolved in 50 ml 2% HNO_3 for elemental analyses. Concentrations of the trace elements V, Mn, Co, Ni, Cu, Zn, Ba and REE were analyzed using a Bruker Aurora M90 ICP-MS at the School of Earth Sciences and Engineering, Nanjing University. The precision of elemental analysis was generally better than ±5%. The REE concentrations of each sample were normalized by Post-Archean Australian Shale (PAAS) values, and the extent of Eu anomalies was expressed using the following equation (Lawrence et al., 2006):

$$\delta Eu = Eu_N/(2/3Sm_N + 1/3Tb_N)$$

where the subscript N means "normalized by PAAS values".

3.2.2. Carbon ($\delta^{13}C$) and oxygen ($\delta^{18}O$) isotope analysis

Eleven bulk carbonate samples (Appendix Table S4-1) and thirty sets of micro-drilled powder for the different types of dolomite (Appendix Table S4-2) were measured for the carbon and oxygen compositions. The $\delta^{13}C$ and $\delta^{18}O$ of carbonate powders were measured using a Thermo Finnigan Delta V Plus isotope ratio mass spectrometer (IRMS) at Nanjing University. All isotope ratios were normalized to the V-PDB standard and reported in per mil (‰). The analytical error (standard error or SE) was <0.1‰ for $\delta^{13}C$ and 0.08‰ for $\delta^{18}O$.

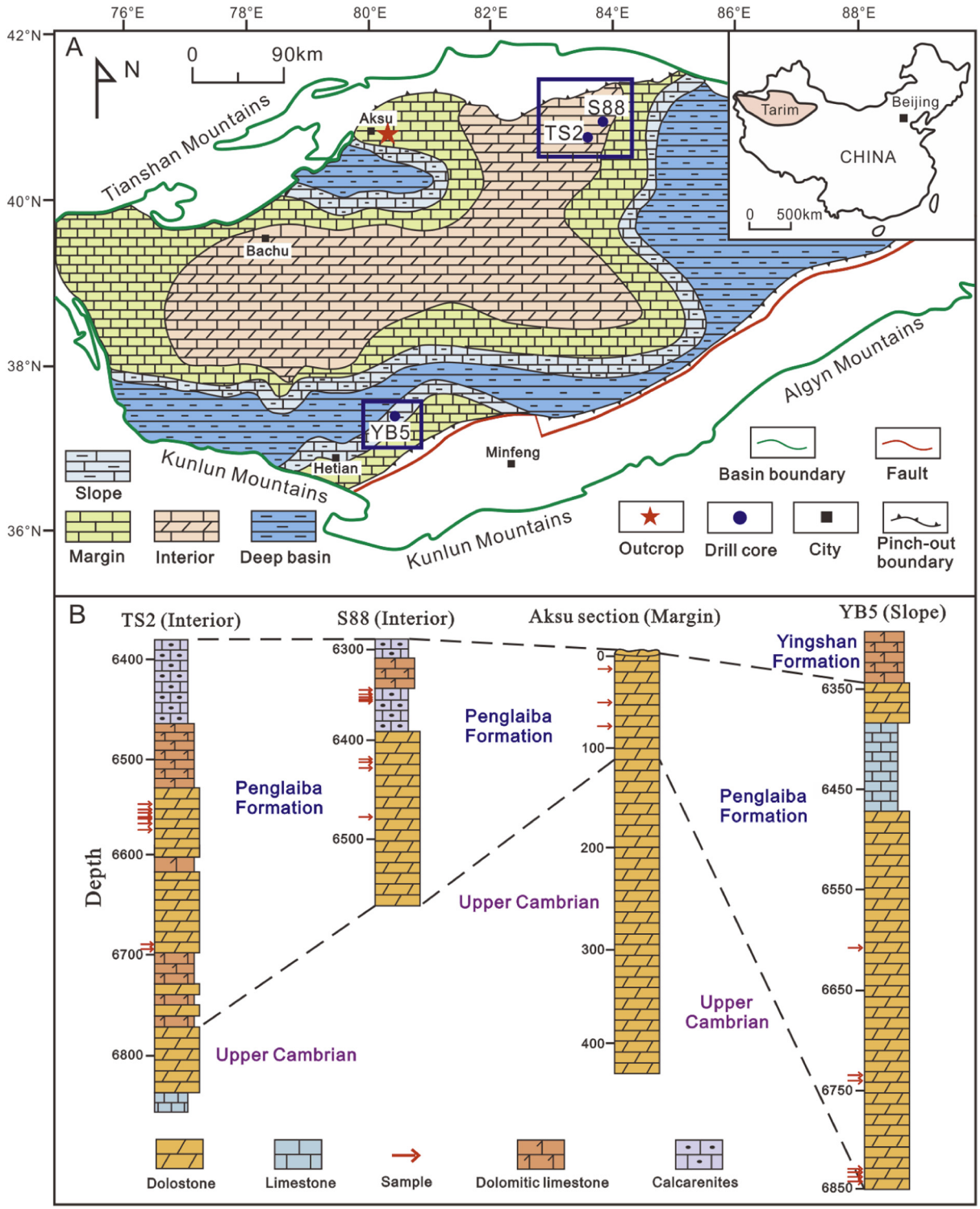

Fig. 1. (A) Sketch map of the Tarim Basin showing sedimentary facies and locations of drilling wells and outcrops (after Gao and Fan, 2015; Guo et al., 2016); (B) stratigraphic correlation of drilling wells and the Aksu outcrop.

3.2.3. Magnesium isotope ($\delta^{26}Mg$) analysis

Twenty-five bulk dolostones and twenty-one micro-drilled power samples for different types of dolomite were measured for Mg isotope compositions. Chemical separation of the Mg fraction for isotope analysis was performed using the procedures described by Hu et al. (2017). After purification, the mass of matrix elements was <1% Mg, and the Mg recovery was >98%. A 1 ppm Mg solution in 2% HNO_3 was measured using a Thermo Fisher Scientific Neptune Plus MC-ICP-MS at Nanjing University. The typical internal precision (2 standard errors or 2 SE) was better than ±0.04‰ for $^{26}Mg/^{24}Mg$ and ±0.02‰ for $^{25}Mg/^{24}Mg$. Based on repeat analysis of multiple geological standards and Mg standard solutions, the long-term external precision and accuracy of the $\delta^{26}Mg$ measurements were better than ±0.10‰ based on repeat measurements of standard samples (Appendix Table S1). The IAPSO seawater and USGS rock standard (DST-2b) were processed with samples via the ion-exchange procedure to monitor the accuracy of

the chemical procedure, and the δ^{26}Mg values of the standards in this study matched the published values within ±0.05‰ (Appendix Table S1).

4. Results

4.1. Petrography and mineralogy

The Penglaiba Formation predominantly comprises dolostones and minor interbedded limestone layers in the upper part of the formation (Fig. 1B). Based on crystal size (Sibley and Gregg, 1987), three types of massive replacement dolomites are identified: (1) fine-crystalline planar-s dolomite, <0.1 mm (D1) (Fig. 2B); (2) medium-crystalline planar-s dolomite, 0.1–0.2 mm (D2) (Fig. 2C, D, E); and (3) coarse-crystalline planar-s dolomite, >0.2 mm (D3) (Fig. 2F). Approximately 30% of the dolostone is composed of multiple types of dolomite, generally D1 and D2 dolomites (Fig. 2C, D). The three types of massive replacement dolomites exhibit similar dull red luminescence under CL, although most medium-coarse dolomites have bright red luminescent rims, which are believed to be diagenetic origin (Fig. 2G, H, I).

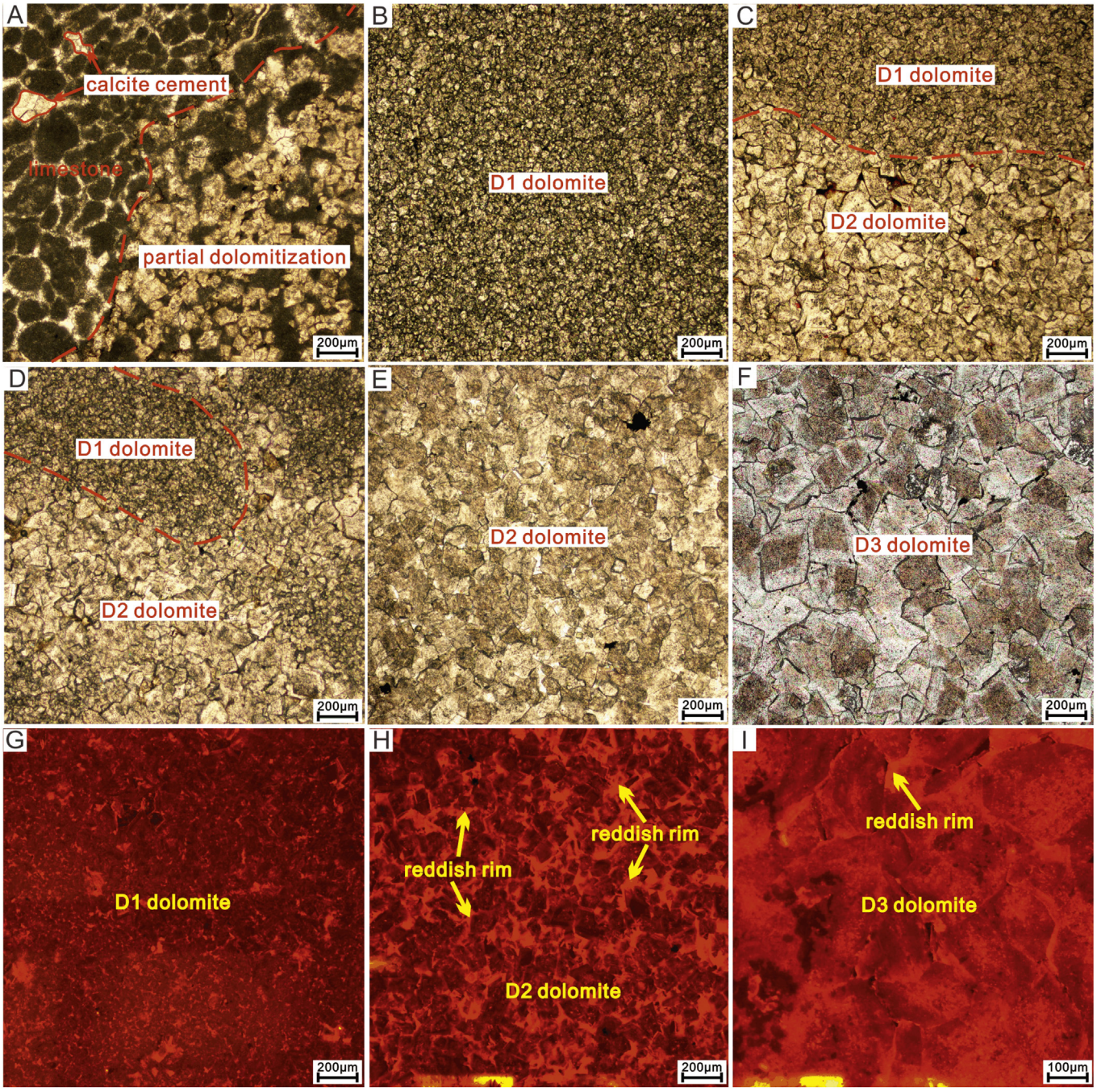

Fig. 2. Photomicrographs showing petrographic characteristics of massive replacement dolomite in the Penglaiba Formation. (A) Partial dolomitization of calcarenite, S88, 6306.88 m, transmitted light; (B) dolomicrite mainly composed of D1 dolomite, pyrite occluded in porosity, S88, 6459.00 m, transmitted light; (C) heterogeneous recrystallization, the bulk dolostone is mainly composed of D1 and D2 dolomite, TS2, 6693.2 m, transmitted light; (D) heterogeneous recrystallization, the dolostone is composed of D1 and D2 dolomite, TS2, 6552.85 m, transmitted light; (E) D2 dolomite, TS2, 6693.20 m, transmitted light; (F) dolostone composed of D3 dolomite, YB5, 6842.15 m, transmitted light; (G) cathodoluminescence photomicrograph of D1 dolomite, S88, 6486.13 m; (H) cathodoluminescence photomicrograph of D2 dolomite, TS2, 6693.20 m; (I) cathodoluminescence photomicrograph of D3 dolomite, YB5, 6839.53 m.

Typical hydrothermal effects in the dolostones include remarkable dolostone decoloration in meter-sized fractures (Fig. 3A, B), vein filling (Fig. 3C, D), silication (Fig. 3E) and dissolution (Fig. 3F, G). Silication bands are composed of interbedded coarse-crystalline planar-s dolomite laminae (LD dolomite) and hydrothermal quartz laminae under microscope (Fig. 3H). The cement dolomite (CD dolomite) rims the dissolution pore (Fig. 3I), with intense reddish luminescence and zonation under CL (Fig. 3J). The vein-filling minerals are mostly composed of calcite and quartz rather than saddle dolomite (Fig. 3C, D). Dissolution, which is associated with the development of secondary porosity, mainly occurs in dolostone that composed of D2 and D3 dolomite (Fig. 3F, G, K). Inter-crystal porosity is absent in dolostone composed of D1 dolomite because the planar-s crystals are tightly interlocked (Fig. 2B).

4.2. Trace elements

For bulk samples, the limestone, fine-crystalline dolostone and medium/coarse-crystalline dolostone have similar average ∑REE concentrations of 3.9 ppm, 6.5 ppm and 3.0 ppm, respectively (Appendix Table S5). For dolomite samples with higher REE contents, the shale-normalized REE patterns are apparently more flat, implying contamination of terrigenous input (Fig. 4A). However, samples with low REE contents show seawater-like LREE-depletion in REE patterns, indicating minimal detrital contribution (Fig. 4A, B). This is supported by the study of Zhao and Jones (2013), who reported that dolostones can record the REE signatures of dolomitization fluids (Zhao and Jones, 2013). Generally, the normalized REE distribution patterns in the limestone, the fine crystalline dolostones and medium-coarse crystalline dolostones are similar, implying a genetic relationship (Fig. 4A).

The dolostones that experienced remarkable hydrothermal alterations, as shown in Fig. 3F and G, display apparent positive Eu anomalies (Fig. 4B) and high Ba contents (Fig. 4C). During the ICP measurement process, Ba and O atoms combine in the plasma and produce $^{137}Ba\cdot^{16}O$, $^{136}Ba\cdot^{17}O$ and $^{135}Ba\cdot^{18}O$, which can interfere with analysis of ^{153}Eu signal, resulting in apparent positive δEu values correlate with Ba contents (Fig. 4D). We interpret that the apparent positive Eu anomalies are analytical artifacts. Previous studies indicate that barite is a typical hydrothermal mineral in lower Ordovician carbonate strata in Tarim Basin, and is presented frequently in dissolution voids/veins (Cai et al., 2008; Jia et al., 2016). The high Ba concentration in dolostones is a signature for hydrothermal activity (Cai et al., 2008; Dong et al., 2013).

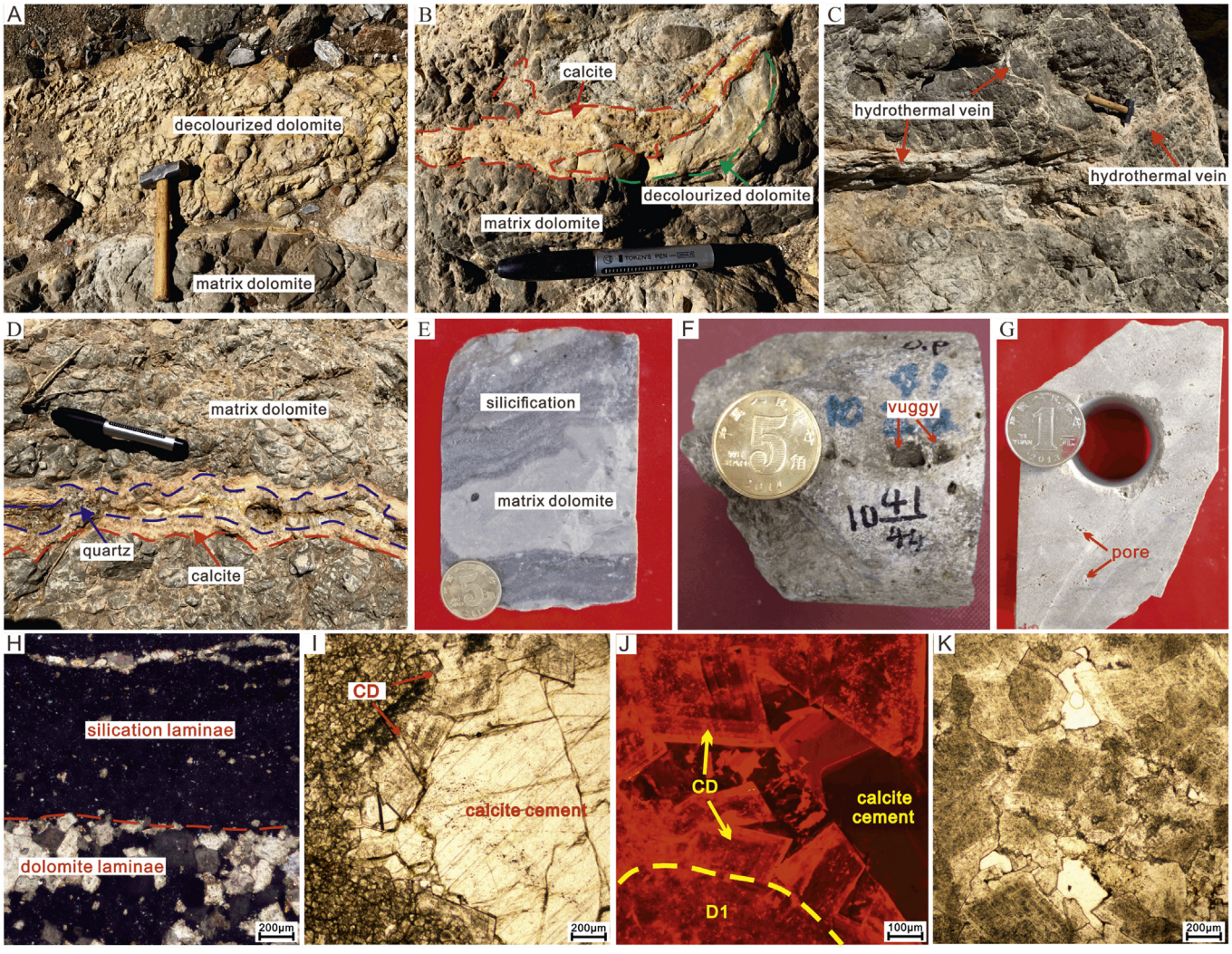

Fig. 3. Photographs showing hydrothermal effects on Penglaiba dolostone. (A) Hydrothermal fluid decolorized the matrix dolomite in a fracture-controlled vein (sample AO-2), Aksu outcrop; (B) hydrothermal fluid decolorized the matrix dolomite, and calcite filled the dissolution vugs (sample AO-3), Aksu outcrop; (C) hydrothermal veins filled with calcite cut the dolostone beds, Aksu outcrop; (D) hydrothermal quartz and calcite filled the vein, Aksu outcrop; (E) silication bands in hand sample YB5, 6842.68 m; (F) dissolution vugs in dolostone mainly composed of D3 dolomite, YB5, 6607.02 m; (G) dissolution pore in bulk dolostone composed of D2 dolomite, TS2, 6692.15 m; (H) interbedded quartz laminae and dolomite laminae in silication bands, YB5, 6739.07 m, plane-polarized light; (I) dissolution pore filled by saddle dolomite cement and block calcite, TS2, 6692.57 m, transmitted light; (J) cathodoluminescence photomicrograph of saddle dolomite rimming around the pore, TS2, 6692.57 m; (K) photomicrograph of (F), dissolution vug.

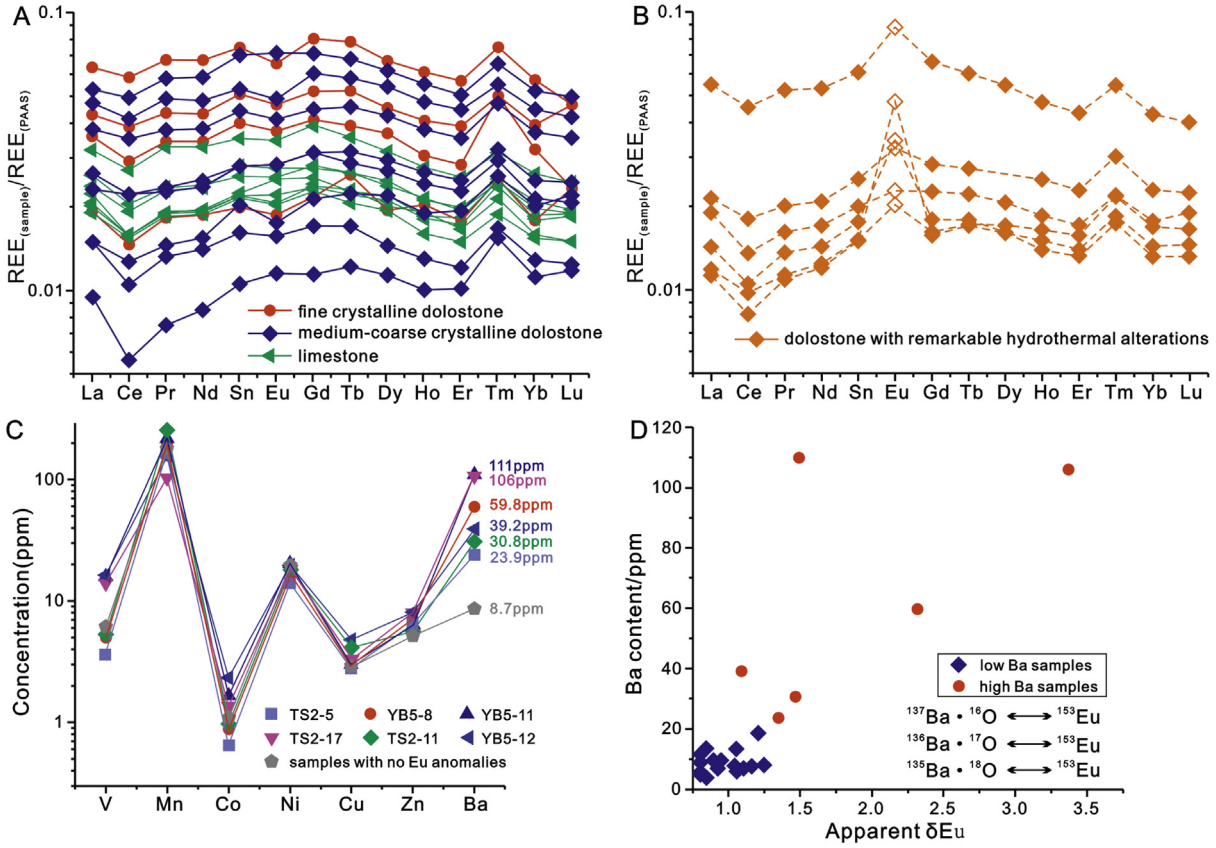

Fig. 4. (A) and (B) PAAS-normalized REE patterns of bulk carbonates from the Penglaiba Formation; (C) comparison of the trace metal element concentrations between samples with or without an Eu anomaly (sample numbers are detailed in Appendix Table S5); (D) cross-plot of Ba contents versus δEu values for bulk dolostone.

4.3. Isotope geochemistry

The limestone and three types of massive replacement dolomites (D1, D2 and D3 dolomite) have a narrow $\delta^{13}C$ range mainly between −2.0‰ and −1.0‰ (Fig. 5A), which is within the range of the published $\delta^{13}C$ values of Tremadocian seawater (−2.5‰ to −0.5‰; Munnecke et al., 2011; Zhang and Munnecke, 2016). Compared to the primary dolostones, the hydrothermally altered dolomites have relatively lower $\delta^{13}C$ values (Fig. 5B).

The $\delta^{18}O$ values of carbonate have a wide span ranging from −9.2‰ to −4.9‰ and display a gradual increase from the limestone to the coarse/medium-crystalline dolomite to the fine-crystalline dolomite (Fig. 5A). The limestones have the most depleted $\delta^{18}O$ values (approximately −9‰), while the fine-crystalline dolomites (D1 dolomite) have the most positive $\delta^{18}O$ values, which range from −7.2‰ to −4.9‰, with an average value of −5.5‰, displaying a $\Delta^{18}O_{dolomite\text{-}calcite}$ fractionation of approximately 3–4‰ (Fig. 5A). The medium-crystalline dolomite (D2 dolomite) and coarse-crystalline dolomite (D3, LD and CD dolomite) have similar and relatively depleted $\delta^{18}O$ values ranging from −8‰ to −7‰ (Fig. 5A).

The three types of massive replacement dolomites (D1, D2 and D3 dolomite) have almost identical $\delta^{26}Mg$ values (average $\delta^{26}Mg = -2.05‰ \pm 0.16‰$, $n = 12$, Appendix Table 2-2) (Fig. 6). The Mg isotope compositions in the bulk samples are relatively homogeneous along the depth profiles of the four sections (average $\delta^{26}Mg = -2.07‰ \pm 0.16‰$, $n = 22$, Appendix Table 2-1) (Fig. 6). The hydrothermal-related dolostone/dolomite, including the decolorized dolostone, dolomite in silication bands (LD dolomite) and CD dolomite, also have similar Mg isotope signatures with the adjacent primary dolomite, considering the analytical uncertainties (Fig. 6) (Appendix Fig. S2), but the $\delta^{26}Mg$ values in the CD dolomite have a relatively wider range (ca. 0.5‰) than those in the discolored dolostone and dolomite in silication bands (LD dolomite) (Fig. 5C, D). Generally, the $\delta^{26}Mg$ values in the different types of dolomites exhibit no covariation with the $\delta^{13}C$ and $\delta^{18}O$ values (Fig. 5C, D). The dolomite samples show a relatively uniform $\delta^{26}Mg$ value of approximately $-2.06‰ \pm 0.20‰$ ($n = 46$).

5. Discussion

5.1. Origin of massive replacement dolomite

Crystallography and sedimentary studies indicated that the fine-crystalline dolomites in marine dolostones generally formed during penecontemporaneous to near-surface dolomitization at moderate ambient temperatures (Machel and Mountjoy, 1986; Sibley and Gregg, 1987), where the solution was oversaturated and the crystallization rate was relatively high (Sibley and Gregg, 1987). Climatic and environmental proxies have indicated that greenhouse conditions prevailed in the early Ordovician with long-standing high temperatures (Trotter et al., 2008; Munnecke et al., 2010), which likely favored the formation of hypersaline seawater in lagoons by evaporation and massive dolomitization (Machel and Mountjoy, 1986). The geochemical signals of the fine-crystalline dolomites and dolomicrites are considered pristine (Banner, 1995). The normalized REE patterns and $\delta^{13}C$ values of the D1 dolomites and dolomicrite in the Penglaiba Formation are consistent with those of the coeval marine limestone (Figs. 4A, 5A), and the average oxygen isotope fractionation between the D1 dolomite and limestone ($\Delta^{18}O_{dolomite\text{-}calcite}$) is approximately 3.5‰, which is comparable with those in syngenetic dolomitization processes (Qing et al., 2001; Kırmacı, 2008; Rameil, 2008) (Fig. 5A). We therefore infer that the D1 dolomite formed via dolomitization of limestone in a syngenetic-penecontemporaneous stage and magnesium in the dolomite was sourced from coeval seawater.

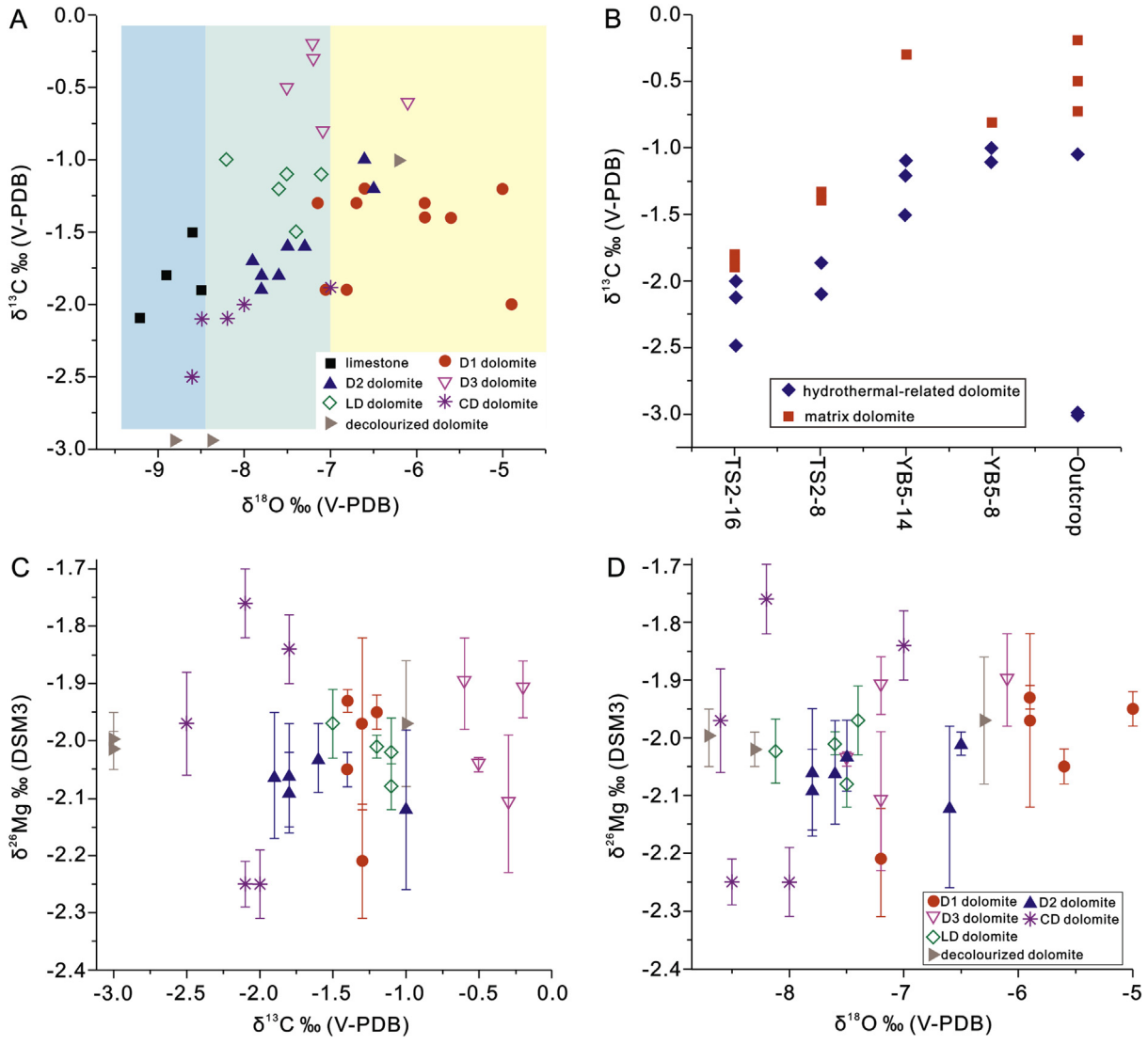

Fig. 5. (A) Cross-plot of $\delta^{13}C$ versus $\delta^{18}O$ values in Penglaiba carbonates; (B) comparison of $\delta^{13}C$ values between hydrothermal-related dolomite and matrix dolomite; (C) cross-plot of $\delta^{13}C$ versus $\delta^{26}Mg$ values in dolomite extracted by microdrilling; (D) cross-plot of $\delta^{18}O$ versus $\delta^{26}Mg$ values in dolomite extracted by microdrilling.

The $\delta^{13}C$ values of the D2 and D3 dolomites are similar to those of carbonates deposited from coeval seawater (Fig. 5A) (Munnecke et al., 2011; Zhang and Munnecke, 2016), and the REE patterns of the D2 and D3 dolomites are also consistent with those in the D1 dolomite and coeval limestones (Fig. 4A). However, the D2 and D3 dolomites have slightly depleted $\delta^{18}O$ values (Fig. 5A), implying diagenetic or hydrothermal effects. CL images show that the D2 and D3 dolomites have overgrowth rims with bright red luminescence around the primary crystals (Fig. 2G, H, I). We propose that the D2 and D3 dolomites originated from the overgrowth and recrystallization of the D1 dolomite in the burial stage and thus the Mg in these dolomites was also ultimately sourced from contemporaneous seawater during initial dolomitization.

5.2. The responses of dolomite Mg isotopes to massive dolomitization

As indicated by the similar $\delta^{26}Mg$ values in the D1, D2 and D3 dolomites, the behavior of Mg isotopes in dolomite can be considered conservative during burial diagenesis. As a result, the Mg isotope compositions in massive replacement dolomite represent original signals that can be used to investigate dolomite Mg isotope variations during massive dolomitization.

It has been suggested that changes in sedimentary environmental factors, such as temperature, hydrodynamic conditions and biological activities, affect the nucleation rate, growth effect of carbonate and mineralization pathways of amorphous calcium carbonate (Gregg and Sibley, 1984; Sibley and Gregg, 1987; Blue et al., 2017; Mavromatis et al., 2017) and consequently affect Mg isotope compositions in calcite (Immenhauser et al., 2010; Mavromatis et al., 2017). A systematic investigation of the Mg isotopes of Carboniferous limestone shows that the $\delta^{26}Mg$ values of different carbonate components in limestone can be heterogeneous (Ma et al., 2017). However, the different types of massive dolomites and bulk dolostones have tight $\delta^{26}Mg$ distribution, with values ranging between −2.15‰ and −1.95‰. Such variation is comparable with external analytical uncertainty for Mg isotope analysis (±0.1‰, Fig. 6), although the massive replacement dolomite in the studied sections formed in the slope (YB5 core), margin (Aksu outcrop) and interior (TS2 and S88 core) of the carbonate platform that are widely separated (Fig. 1A). This implies that the dolomitization fluids in the carbonate platform were homogeneous in Mg isotopes. Additionally, dolomitization may have homogenized the original variabilities in Mg isotopes in the precursor materials.

Previous works indicated that dolostones in the early Paleozoic in the Tarim Basin mainly formed via reflux dolomitization processes (Guo et al., 2016; Du et al., 2018). The exchange of seawater with carbonate in the platform is thought to be adequate via continued reflux circulation, to sustain the dolomitization process. Unhindered

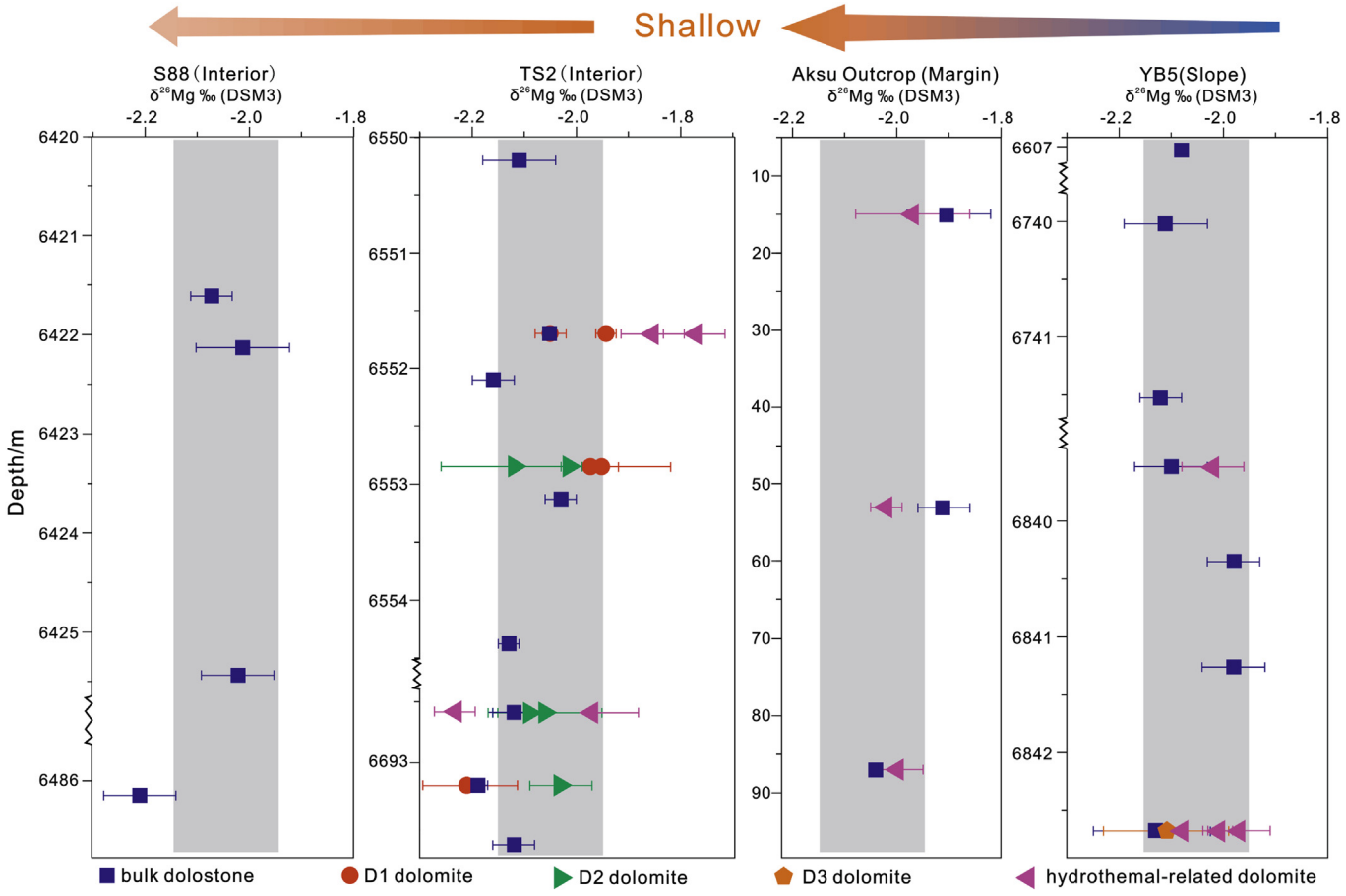

Fig. 6. A summary of δ^{26}Mg values in various dolomite/dolostone samples along the depth profiles of the studied sections.

hydrologic circulation of hypersaline water kept the chemistry of the porewater in equilibrium with that of the seawater and resulted in homogeneous δ^{26}Mg values in the dolomite. Furthermore, despite the geographic separation, the Mg isotope ratios of the dolomite in the Tarim Basin are comparable with the published δ^{26}Mg values of coeval dolostones (Watts Bight and Boat Harbour Formation) in eastern Laurentia (−1.80‰ to −2.27‰, Azmy et al., 2013).

Based on the discussions above, we suggest that the early diagenesis system associated with massive dolomitization was "seawater buffered", according to the classification of diagenesis systems of Higgins et al. (2018). In the burial stage, the fluid in sediments was expelled by compaction, and the diagenesis system transformed from "seawater buffered" to "sediment buffered" along the depth profile (Ahm et al., 2018; Higgins et al., 2018). However, due to massive dolomitization in the penecontemporaneous stage, the sediment column was mainly composed of dolomite; consequently, dolomite controlled the Mg mass balance in the later "sediments-buffered" system, and the remnant porewater could not reset the bulk dolomite Mg isotope compositions. Therefore, D1, D2 and D3 dolomite have relatively homogeneous Mg isotope compositions, demonstrating that dolomite Mg isotopes were conservative during burial diagenesis (Geske et al., 2012; Azmy et al., 2013; Hu et al., 2017).

5.3. Behavior of Mg isotopes during hydrothermal reworking of dolomites

Previous studies on hydrothermal activities have suggested that fluid geochemistry is the primary control of Mg isotope compositions in hydrothermal carbonate (Lavoie et al., 2014; Walter et al., 2015). In this study, the hydrothermal effects in Penglaiba dolostone are conspicuous and include decolorization (Fig. 3A, B), dissolution (Fig. 3F, G, K), vein/vug-filling precipitates, such as calcite (Fig. 3C, D), quartz (Fig. 3D, E, H), CD dolomite precipitation (Fig. 3H, J), and high Ba contents in the bulk dolostone (Fig. 4B); thus, we expected that the hydrothermally affected dolomites might have different δ^{26}Mg values than the massive dolomite. However, as shown in Fig. 6, no distinction can be detected in the Mg isotope compositions of these dolomites. For comparison, previous studies show that the δ^{26}Mg values of hydrothermal dolomite in typical hydrothermal systems have a wide range from −2.5‰ to 0‰ (Fig. 7), and the corresponding variations in Mg isotope signals of hydrothermal fluid were caused by fluid migration and water-rock interactions (Lavoie et al., 2014; Walter et al., 2015).

We speculate that the Mg isotope mass balance in water-rock interactions was dominated by the primary dolostone and that the Mg contents in the hydrothermal fluid in the Penglaiba Formation were insignificant relative to existing dolostones. This is confirmed by field observation that saddle dolomite is absent in most vein-filling minerals, which are instead composed of calcite and quartz (Fig. 3). This indicates that the hydrothermal fluid was almost Mg-free. Experiments suggest that hydrothermal dissolution of dolomite does not produce secondary minerals, and does not incur obvious Mg exchanges during the fluid-rock interactions (Perez-Fernandez et al., 2017). Therefore we do not expect hydrothermal alterations of massive dolostones to cause Mg isotope fractionations in dolomite. Although the CD dolomite that precipitated in closed pore systems had slightly different δ^{26}Mg values than the bulk dolostone (Fig. 5C, D), this difference does not shift the Mg isotope compositions in the bulk dolostone, because of the negligible amount of CD dolomite in dolostones. In summary, the impacts of hydrothermal alterations on the dolomite Mg isotopes should be limited, and the hydrothermally altered dolostones have Mg isotope compositions similar to the well-preserved dolostones (Figs. 5C, D, 6). Notably, the

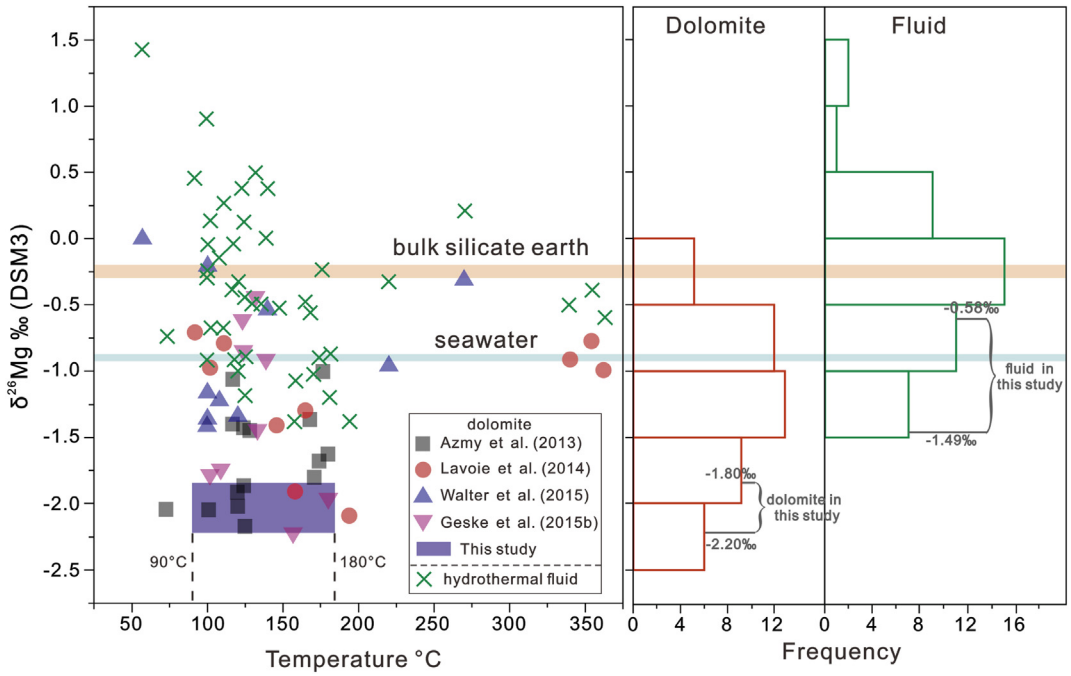

Fig. 7. Compilation of δ^{26}Mg values of high-temperature dolomite from different hydrothermal systems. The temperature range from 90 °C to 180 °C represents the homogenization temperatures of two-phase aqueous inclusions in the vein/vug-filling minerals of the Penglaiba Formation (Cai et al., 2008; Dong et al., 2013; Du et al., 2018).

hydrothermally affected dolomites in the Penglaiba Formation are not the same as typical hydrothermal dolomites in terms of genesis and geologic occurrence (Davies and Smith, 2006; Mansurbeg et al., 2016).

Zircons in the hydrothermal veins of the Penglaiba Formation have a weighted mean ^{206}Pb-^{238}U age of 290.5 ± 2.9 Ma, indicating that the hydrothermal events coincided with the massive magmatism that associated with the Hercynian Orogeny in the early Permian (Dong et al., 2013). Because the mantle reserves vast amounts of carbon with depleted isotopic signals, the exsolution of gas via magma activities results in high CO_2 concentrations with low $\delta^{13}C_{CO2}$ values in hydrothermal fluids (Bianchini and Natali, 2017). Unlike the relatively robust Mg isotopes during hydrothermal alteration, the δ^{13}C values of the hydrothermally affected dolomite are, to some extent, relatively more depleted than those of the primary dolomite due to the participation of mantle-sourced carbon in the hydrothermal fluids (Fig. 5B).

5.4. The potential of dolomite Mg isotopes as a proxy for seawater chemistry

The consistent Mg isotope data in this study indicate that there had been adequate Mg isotope exchange between dolomite and coeval seawater during massive dolomitization for the Penglaiba Formation, resulting in equilibrium Mg isotope distribution between seawater and dolomite irrespective of the sedimentary environments. This interpretation is consistent with the long residence time (~13 Ma, Berner and Berner, 1996) and large buffer capacity of Mg in seawater. Li et al. (2015) calculated the δ^{26}Mg curves of seawater and massive syndepositional dolomite throughout the Phanerozoic based on a static isotope mass balance model and the variation in dolomitization intensity over geological history. As an overview, the reported δ^{26}Mg values of massive dolomite in the Mesozoic-Paleozoic roughly match the modeled curve for syndepositional dolomite (Fig. 8), including those in the middle Cambrian (Peng et al., 2016), lower Ordovician (Azmy et al., 2013), Mississippian (Jacobson et al., 2010), Anisian in the Middle Triassic (Hu et al., 2017). The δ^{26}Mg values of Penglaiba Formation are also consistent with the modeled curve. This implies that massive dolomite can be used as an archive for inferring the Mg isotope composition of seawater.

It is important to note that the δ^{26}Mg values measured from the Penglaiba Formation still cover a substantial range (i.e., ±0.2‰), therefore the precision of seawater δ^{26}Mg reconstruction based on massive dolostones would be limited (±0.2‰), if without further constraints. Such observed range in δ^{26}Mg values from dolostones may be due to the existence of small-scale Mg isotope variability in the dolomitization system in the Tarim basin during the deposition of the Penglaiba Formation. Two published studies have documented small-scale seawater Mg isotope variations in time and space. First, the δ^{26}Mg profiles of

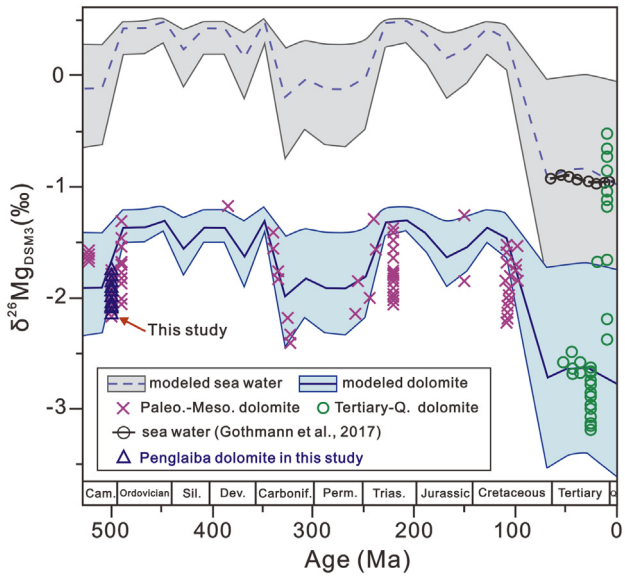

Fig. 8. Comparison of measured δ^{26}Mg values of dolomite and the proposed δ^{26}Mg curves for massive dolomite and seawater during the Phanerozoic. The Mg isotope compositions of Phanerozoic sedimentary dolomite were reported by Jacobson et al. (2010), Geske et al. (2012), Azmy et al. (2013), Fantle and Higgins (2014), Geske et al. (2015a, 2015b), Peng et al. (2016), Hu et al. (2017), Higgins et al. (2018) and Bialik et al. (2018). The δ^{26}Mg values of Cenozoic seawater of Gothmann et al. (2017) were deduced through the measured δ^{26}Mg values of fossil corals (Gothmann et al., 2017).

ca. 635 Ma cap dolostones exhibit variabilities caused by severe seawater stratification (Liu et al., 2014). Second, rhythmic variations in the δ^{26}Mg values of mid-Cretaceous dolomite sequence were caused by dolomitization in a restricted basin with episodic seawater replenishment (Bialik et al., 2018). It is possible that the low-density sampling of dolostones from the Penglaiba Formation in the basin missed the spatial- and temporal Mg isotope variability on smaller scales. Indeed, essentially all previous studies that discussed the effects of diagenesis on Mg isotopes in dolomite were focused on Mg isotope variability on a scale of <100 m (Fantle and Higgins, 2014; Geske et al., 2015b; Huang et al., 2015; Ahm et al., 2018; Higgins et al., 2018). These studies, however, invoke evolution of pore fluid isotope compositions in various diffusion-limited scenarios for Mg, which are fundamentally incompatible with development of the giant massive dolostones units such as the Penglaiba Formation, which require tremendously large supply of Mg. The simple and straightforward interpretation of Mg isotope signature of massive dolomite is that the dolomite was "seawater buffered", therefore we argue that the δ^{26}Mg ancient seawater derived from massive dolostones would be accurate, although it may not be very precise.

6. Conclusions

Petrographic features and multiple geochemical tracers enabled us to identify multiple generations of dolomite in the Penglaiba Formation in the Tarim Basin and characterize the Mg isotope behaviors of these processes. As indicated by C-O isotopes and REE-normalized patterns, the Tremadocian coeval seawater responded to massive dolomitization. The internal heterogeneities in the carbonate platform were not tightly associated with dolomite Mg isotope ratios, and the diagenetic system during ancient massive dolomitization was "fluid buffered". Thus, the dolomite that precipitated in the different settings of the carbonate platform had similar Mg isotope compositions and was in isotopic equilibrium with the seawater. During the burial stage, hydrothermal alterations occurred widely in the Penglaiba dolostone and were characterized by rock decoloration, crystal recrystallization, dissolution and vein/pore filling and a high Ba content in the bulk dolostone. However, the Mg isotope compositions of the dolostone do not show correlations with diagenetic indicators, demonstrating that the dolomite Mg isotopes were robust against hydrothermal alteration. This study supports the idea that dolomite can potentially serve as an archive of coeval seawater Mg isotope signals. It must be noted that the dolomites we investigated in this study formed via massive dolomitization in a shallow carbonate platform rather than in deep marine deposits.

Acknowledgments

This manuscript benefits from constructive comments from an anonymous reviewer. And we also thank Prof. Brian Jones for the highly efficient editorial handling and constructive comments. This study is supported by the National Science Foundation of China (grants 41473002, 41561144002, and 41622301 to W. Li, 41830425 to W. Hu) and the program B for Outstanding Ph.D. Candidates of Nanjing University (201801B040).

Appendix A. Supplementary data

Supplementary data to this article can be found online at https://doi.org/10.1016/j.sedgeo.2018.12.007.

References

Ahm, A.-S.C., Bjerrum, C.J., Blättler, C.L., Swart, P.K., Higgins, J.A., 2018. Quantifying early marine diagenesis in shallow-water carbonate sediments. Geochimica et Cosmochimica Acta 236, 140–159.

Azmy, K., Lavoie, D., Wang, Z., Brand, U., Al-Aasm, I., Jackson, S., Girard, I., 2013. Magnesium-isotope and REE compositions of Lower Ordovician carbonates from eastern Laurentia: implications for the origin of dolomites and limestones. Chemical Geology 356, 64–75.

Banner, J.L., 1995. Application of the trace element and isotope geochemistry of strontium to studies of carbonate diagenesis. Sedimentology 42, 805–824.

Berner, E.K., Berner, R.A., 1996. Global Environment: Water, Air and Geochemical Cycles. Prentice Hall, Upper Saddle River, NJ.

Bialik, O.M., Wang, X., Zhao, S., Waldmann, N.D., Frank, R., Li, W., 2018. Mg isotope response to dolomitization in hinterland-attached carbonate platforms: outlook of δ^{26}Mg as a tracer of basin restriction and seawater Mg/Ca ratio. Geochimica et Cosmochimica Acta 235, 189–207.

Bianchini, G., Natali, C., 2017. Carbon elemental and isotopic composition in mantle xenoliths from Spain: insights on sources and petrogenetic processes. Lithos 272-273, 84–91.

Blättler, C.L., Miller, N.R., Higgins, J.A., 2015. Mg and Ca isotope signatures of authigenic dolomite in siliceous deep-sea sediments. Earth and Planetary Science Letters 419, 32–42.

Blue, C.R., Giuffre, A., Mergelsberg, S., Han, N., De Yoreo, J.J., Dove, P.M., 2017. Chemical and physical controls on the transformation of amorphous calcium carbonate into crystalline $CaCO_3$ polymorphs. Geochimica et Cosmochimica Acta 196, 179–196.

Cai, C., Li, K., Li, H., Zhang, B., 2008. Evidence for cross formational hot brine flow from integrated $^{87}Sr/^{86}Sr$, REE and fluid inclusions of the Ordovician veins in Central Tarim, China. Applied Geochemistry 23, 2226–2235.

Chanda, P., Fantle, M.S., 2017. Quantifying the effect of diagenetic recrystallization on the Mg isotopic composition of marine carbonates. Geochimica et Cosmochimica Acta 204, 219–239.

Davies, G.R., Smith, L.B., 2006. Structurally controlled hydrothermal dolomite reservoir facies: An overview. American Association of Petroleum Geologists Bulletin 90, 1641–1690.

Dong, S., Chen, D., Qing, H., Zhou, X., Wang, D., Guo, Z., Jiang, M., Qian, Y., 2013. Hydrothermal alteration of dolostones in the Lower Ordovician, Tarim Basin, NW China: multiple constraints from petrology, isotope geochemistry and fluid inclusion microthermometry. Marine and Petroleum Geology 46, 270–286.

Du, Y., Fan, T., Machel, H.G., Gao, Z., 2018. Genesis of Upper Cambrian-Lower Ordovician dolomites in the Tahe Oilfield, Tarim Basin, NW China: several limitations from petrology, geochemistry, and fluid inclusions. Marine and Petroleum Geology 91, 43–70.

Fantle, M.S., Higgins, J., 2014. The effects of diagenesis and dolomitization on Ca and Mg isotopes in marine platform carbonates: implications for the geochemical cycles of Ca and Mg. Geochimica et Cosmochimica Acta 142, 458–481.

Gao, Z., Fan, T., 2014. Intra-platform tectono-sedimentary response to geodynamic transition along the margin of the Tarim Basin, NW China. Journal of Asian Earth Sciences 96, 178–193.

Gao, Z., Fan, T., 2015. Carbonate platform-margin architecture and its influence on Cambrian-Ordovician reef-shoal development, Tarim Basin, NW China. Marine and Petroleum Geology 68, 291–306.

Geske, A., Zorlu, J., Richter, D.K., Buhl, D., Niedermayr, A., Immenhauser, A., 2012. Impact of diagenesis and low grade metamorphosis on isotope (δ^{26}Mg, δ^{13}C, δ^{18}O and $^{87}Sr/^{86}Sr$) and elemental (Ca, Mg, Mn, Fe and Sr) signatures of Triassic sabkha dolomites. Chemical Geology 332-333, 45–64.

Geske, A., Goldstein, R.H., Mavromatis, V., Richter, D.K., Buhl, D., Kluge, T., John, C.M., Immenhauser, A., 2015a. The magnesium isotope (δ^{26}Mg) signature of dolomites. Geochimica et Cosmochimica Acta 149, 131–151.

Geske, A., Lokier, S., Dietzel, M., Richter, D.K., Buhl, D., Immenhauser, A., 2015b. Magnesium isotope composition of sabkha porewater and related (Sub-)Recent stoichiometric dolomites, Abu Dhabi (UAE). Chemical Geology 393-394, 112–124.

Gothmann, A.M., Stolarski, J., Adkins, J.F., Higgins, J.A., 2017. A Cenozoic record of seawater Mg isotopes in well-preserved fossil corals. Geology 45, 1039–1042.

Gregg, J.M., Sibley, D.F., 1984. Epigenetic dolomitization and the origin of xenotopic dolomite texture. Journal of Sedimentary Research 54, 908–931.

Guo, C., Chen, D., Qing, H., Dong, S., Li, G., Wang, D., Qian, Y., Liu, C., 2016. Multiple dolomitization and later hydrothermal alteration on the Upper Cambrian-Lower Ordovician carbonates in the northern Tarim Basin, China. Marine and Petroleum Geology 72, 295–316.

Higgins, J.A., Schrag, D.P., 2012. Records of Neogene seawater chemistry and diagenesis in deep-sea carbonate sediments and pore fluids. Earth and Planetary Science Letters 357-358, 386–396.

Higgins, J.A., Schrag, D.P., 2015. The Mg isotopic composition of Cenozoic seawater – evidence for a link between Mg-clays, seawater Mg/Ca, and climate. Earth and Planetary Science Letters 416, 73–81.

Higgins, J.A., Blättler, C.L., Lundstrom, E.A., Santiago-Ramos, D.P., Akhtar, A.A., Crüger Ahm, A.S., Bialik, O., Holmden, C., Bradbury, H., Murray, S.T., Swart, P.K., 2018. Mineralogy, early marine diagenesis, and the chemistry of shallow-water carbonate sediments. Geochimica et Cosmochimica Acta 220, 512–534.

Hu, Z., Hu, W., Wang, X., Lu, Y., Wang, L., Liao, Z., Li, W., 2017. Resetting of Mg isotopes between calcite and dolomite during burial metamorphism: outlook of Mg isotopes as geothermometer and seawater proxy. Geochimica et Cosmochimica Acta 208, 24–40.

Huang, K., Shen, B., Lang, X., Tang, W., Peng, Y., Ke, S., Kaufman, A.J., Ma, H., Li, F., 2015. Magnesium isotopic compositions of the Mesoproterozoic dolostones: implications for Mg isotopic systematics of marine carbonates. Geochimica et Cosmochimica Acta 164, 333–351.

Huang, K.J., Teng, F.Z., Shen, B., Xiao, S., Lang, X., Ma, H.R., Fu, Y., Peng, Y., 2016. Episode of intense chemical weathering during the termination of the 635 Ma Marinoan glaciation. Proceedings of the National Academy of Sciences of the United States of America 113, 14904–14909.

Immenhauser, A., Buhl, D., Richter, D., Niedermayr, A., Riechelmann, D., Dietzel, M., Schulte, U., 2010. Magnesium-isotope fractionation during low-Mg calcite precipita-

tion in a limestone cave–field study and experiments. Geochimica et Cosmochimica Acta 74, 4346–4364.
Jacobson, A.D., Zhang, Z., Lundstrom, C., Huang, F., 2010. Behavior of Mg isotopes during dedolomitization in the Madison Aquifer, South Dakota. Earth and Planetary Science Letters 297, 446–452.
Jia, L., Cai, C., Jiang, L., Zhang, K., Li, H., Zhang, W., 2016. Petrological and geochemical constraints on diagenesis and deep burial dissolution of the Ordovician carbonate reservoirs in the Tazhong area, Tarim Basin, NW China. Marine and Petroleum Geology 78, 271–290.
Kırmacı, M.Z., 2008. Dolomitization of the late Cretaceous–Paleocene platform carbonates, Gölköy (Ordu), eastern Pontides, NE Turkey. Sedimentary Geology 203, 289–306.
Lavoie, D., Jackson, S., Girard, I., 2014. Magnesium isotopes in high-temperature saddle dolomite cements in the lower Paleozoic of Canada. Sedimentary Geology 305, 58–68.
Lawrence, M.G., Greig, A., Collerson, K.D., Kamber, B.S., 2006. Rare earth element and yttrium variability in south east Queensland waterways. Aquatic Geochemistry 12, 39–72.
Li, W., Beard, B.L., Li, C., Xu, H., Johnson, C.M., 2015. Experimental calibration of Mg isotope fractionation between dolomite and aqueous solution and its geological implications. Geochimica et Cosmochimica Acta 157, 164–181.
Lin, B., Zhang, X., Xu, X., Yuan, J., Neng, Y., Zhu, J., 2015. Features and effects of basement faults on deposition in the Tarim Basin. Earth-Science Reviews 145, 43–55.
Liu, C., Wang, Z., Raub, T.D., Macdonald, F.A., Evans, D.A.D., 2014. Neoproterozoic cap-dolostone deposition in stratified glacial meltwater plume. Earth and Planetary Science Letters 404, 22–32.
Ma, H., Xu, Y., Huang, K., Sun, Y., Ke, S., Peng, Y., Lang, X., Yan, Z., Shen, B., 2017. Heterogeneous Mg isotopic composition of the early Carboniferous limestone: implications for carbonate as a seawater archive. Acta Geochimica 37, 1–18.
Machel, H.G., Mountjoy, E.W., 1986. Chemistry and environments of dolomitization — a Reappraisal. Earth Science Reviews 23, 175–222.
Mansurbeg, H., Morad, D., Othman, R., Morad, S., Ceriani, A., Al-Aasm, I., Kolo, K., Spirov, P., Proust, J.N., Preat, A., Koyi, H., 2016. Hydrothermal dolomitization of the Bekhme formation (Upper Cretaceous), Zagros Basin, Kurdistan Region of Iraq: record of oil migration and degradation. Sedimentary Geology 341, 147–162.
Mavromatis, V., Purgstaller, B., Dietzel, M., Buhl, D., Immenhauser, A., Schott, J., 2017. Impact of amorphous precursor phases on magnesium isotope signatures of Mg-calcite. Earth and Planetary Science Letters 464, 227–236.
Munnecke, A., Calner, M., Harper, D.A.T., Servais, T., 2010. Ordovician and Silurian sea–water chemistry, sea level, and climate: a synopsis. Palaeogeography, Palaeoclimatology, Palaeoecology 296, 389–413.
Munnecke, A., Zhang, Y., Liu, X., Cheng, J., 2011. Stable carbon isotope stratigraphy in the Ordovician of South China. Palaeogeography, Palaeoclimatology, Palaeoecology 307, 17–43.
Nie, S., 1991. Paleoclimatic and paleomagnetic constraints on the Paleozoic reconstructions of south China, north China and Tarim. Tectonophysics 196, 279–308.
Peng, Y., Shen, B., Lang, X.-G., Huang, K.-J., Chen, J.-T., Yan, Z., Tang, W.-b., Ke, S., Ma, H.-R., Li, F.-B., 2016. Constraining dolomitization by Mg isotopes: a case study from partially dolomitized limestones of the middle Cambrian Xuzhuang Formation, North China. Geochemistry, Geophysics, Geosystems 17, 1109–1129.
Perez-Fernandez, A., Berninger, U.N., Mavromatis, V., Pogge von Strandmann, P.A.E., Oelkers, E.H., 2017. Ca and Mg isotope fractionation during the stoichiometric dissolution of dolomite at temperatures from 51 to 126 °C and 5 bars CO_2 pressure. Chemical Geology 467, 76–88.
Qing, H., Bosence, D.W.J., Rose, E.P.E., 2001. Dolomitization by penesaline sea water in Early Jurassic peritidal platform carbonates, Gibraltar, western Mediterranean. Sedimentology 48, 153–163.
Rameil, N., 2008. Early diagenetic dolomitization and dedolomitization of Late Jurassic and earliest Cretaceous platform carbonates: a case study from the Jura Mountains (NW Switzerland, E France). Sedimentary Geology 212, 70–85.
Riechelmann, S., Mavromatis, V., Buhl, D., Dietzel, M., Eisenhauer, A., Immenhauser, A., 2016. Impact of diagenetic alteration on brachiopod shell magnesium isotope (δ^{26}Mg) signatures: experimental versus field data. Chemical Geology 440, 191–206.
Rollion-Bard, C., Saulnier, S., Vigier, N., Schumacher, A., Chaussidon, M., Lécuyer, C., 2016. Variability in magnesium, carbon and oxygen isotope compositions of brachiopod shells: implications for paleoceanographic studies. Chemical Geology 423, 49–60.
Sibley, D.F., Gregg, J.M., 1987. Classification of dolomite rock textures. Journal of Sedimentary Research 57, 967–975.
Trotter, J.A., Williams, I.S., Barnes, C.R., Lecuyer, C., Nicoll, R.S., 2008. Did cooling oceans trigger Ordovician biodiversification? Evidence from conodont thermometry. Science 321, 550–554.
Walter, B.F., Immenhauser, A., Geske, A., Markl, G., 2015. Exploration of hydrothermal carbonate magnesium isotope signatures as tracers for continental fluid aquifers, Schwarzwald mining district, SW Germany. Chemical Geology 400, 87–105.
Warren, J., 2000. Dolomite: occurrence, evolution and economically important associations. Earth-Science Reviews 52, 1–81.
Wilkinson, B.H., Algeo, T.J., 1989. Sedimentary carbonate record of calcium-magnesium cycling. American Journal of Science 289, 1158–1194.
Zhang, Y., Munnecke, A., 2016. Ordovician stable carbon isotope stratigraphy in the Tarim Basin, NW China. Palaeogeography, Palaeoclimatology, Palaeoecology 458, 154–175.
Zhao, H., Jones, B., 2013. Distribution and interpretation of rare earth elements and yttrium in Cenozoic dolostones and limestones on Cayman Brac, British West Indies. Sedimentary Geology 284-285, 26–38.